J. Fluid Mech. (1989), *vol.* 205, *pp.* 553–571
Printed in Great Britain

Stability of periodic arrays of cylinders across the stream by direct simulation

By P. SINGH[1], PH. CAUSSIGNAC[2], A. FORTES[3], D. D. JOSEPH[1] AND T. LUNDGREN[1]

[1] Department of Aerospace Engineering and Mechanics, University of Minnesota, 107 Akerman Hall, Minneapolis, MN 55455, USA

[2] Department of Mathematics, Swiss Federal Institute of Technology, CH-1015 Lausanne, Switzerland

[3] Department of Mechanical Engineering, University of Brasilia, 70910 Brasilia DF, Brasil

(Received 6 October 1988)

We treat the problem of the stability of an infinite horizontal array of cylinders, spaced periodically, by a direct numerical simulation of the Navier–Stokes equations for steady flow at Reynolds numbers less than or equal to 100. We find that the only stable configuration for the array is one with equal spacing between cylinders and all cylinders lying on a line perpendicular to the flow. The array is found to be stable under displacements of the cylinders perpendicular and parallel to the array. We say a perturbation is stable when it gives rise to a force which acts to restore the original stable configuration. Our results are consistent with experiments in which spheres were confined by the sidewalls of a fluidized bed to move in two dimensions. As a secondary issue we consider the variation with parameters of the length and width of wakes behind cylinders.

1. Introduction

Experiments on fluidization with water of spherical particles falling against gravity in columns of rectangular cross-section are described in the recent papers by Fortes, Joseph & Lundgren (1987) and Joseph *et al.* (1987). All of these experiments are dominated by inertial effects associated with wakes. Two local mechanisms are involved: drafting, and kissing, and tumbling into stable cross-stream arrays. Drafting and kissing are the rearrangement mechanisms in which one sphere is captured in the wake of the other. A sphere in the wake of another sphere is accelerated by the pressure deficit until the two spheres kiss. The kissing spheres are aligned with the stream. The streamwise alignment is massively unstable and the kissing spheres tumble into more stable cross-stream pairs or doublets which can aggregate into larger relatively stable horizontal arrays. The stability of cross-stream arrays in beds of spheres constrained to move in two dimensions is amazing. A somewhat weaker form of cooperative motion of cross-stream arrays of rising spheres is found in beds of square cross-section where the spheres may move freely in three dimensions.

Experiments using cylinders of different length-to-diameter ratios were also carried out. All objects float with their broad side perpendicular to the stream, broadside on. The broadside-on position of particles is due to a turning couple at the front of bodies which is of the same nature as the couple that turns canoes broadside on in a stream or cause an aircraft to stall, and an explanation can be given from

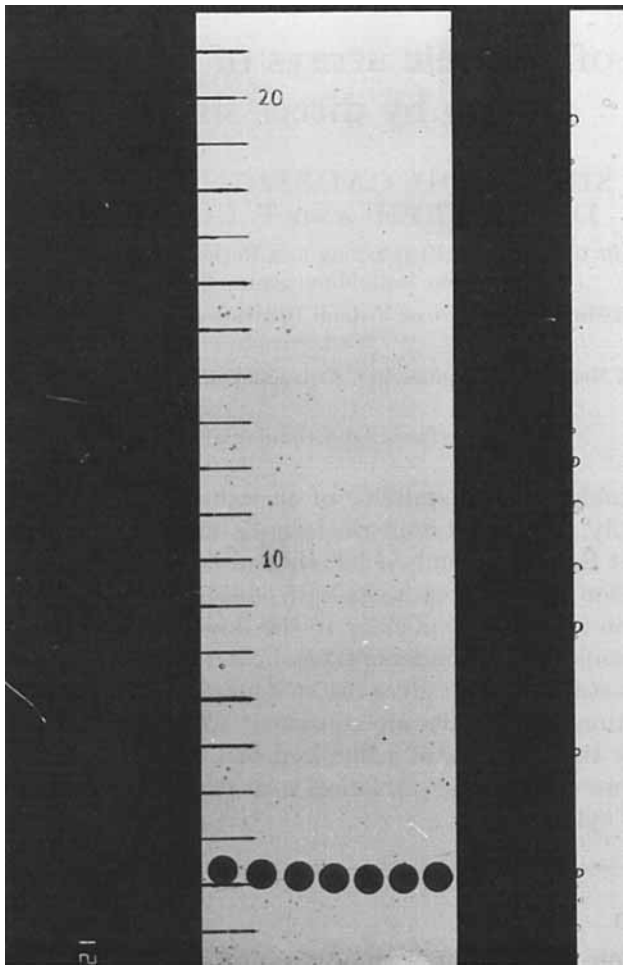

FIGURE 1. Stable cross-stream array of plastic spheres, $D = 6.35$ mm, $R = 350$. The flow is against gravity. The spheres are stationary except for sidewise rocking due to vortex shedding.

potential flow. This explanation is formed in terms of the natural hydrodynamic couple produced at the stagnation points in the flow around a long body, which turns the body so that its broad side faces the stream (cf. Joseph *et al.* 1987, §5). Kissing spheres are a composite body equivalent to a long cylinder; they tumble because of the turning couple on the composite body. Then they separate. The effect of drafting, kissing and tumbling is such as to bring the line of centres between two spheres into the cross-stream position, the other positions are basically unstable because they are prey to wake interactions and drafting. The effects of wakes behind spheres and of turning couples on long bodies lead to a kind of dynamical justification of one-dimensional mathematical treatments, e.g. Wallis (1969), which might at first be thought to be merely convenient.

The numerical simulation presented in this paper introduces a novel method of testing the stability of cross-stream arrays of spheres observed in beds of narrow gap in which the spheres are constrained to move in two dimensions; see figures 1 and 2 in this paper and figures 6, 9 and 15 in Fortes *et al.* (1987). The one-dimensional structure of a fluidized bed of spheres constrained to move in two dimensions

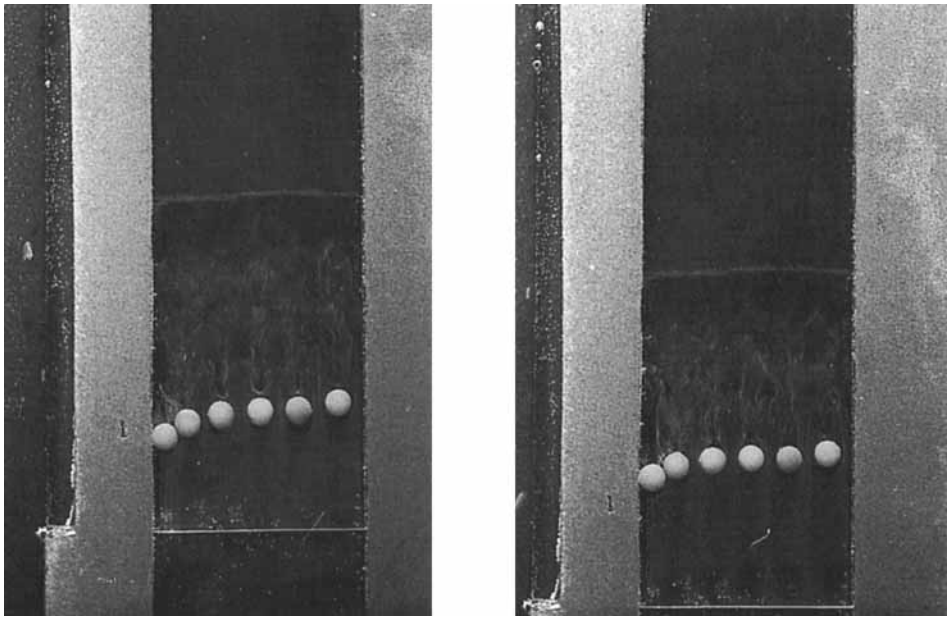

FIGURE 2. Flow visualization of a stable cross-stream array of plastic spheres using hydrogen bubbles, $R = 305$.

is apparent in figure 3, in figures 11, 12 and 15 in Fortes *et al.*, and in figure 15 of Joseph *et al.* (1987).

The same mechanisms, drafting, kissing and tumbling, which lead to flow-induced anisotropy favouring cross-stream alignment in two-dimensional beds are also at work in three dimensions. Drafting and kissing are local effects which are important whenever the velocity of the water relative to the spheres is large enough to produce a strong wake. Turning couples on long bodies, for example on kissing spheres, are also inertial effects independent of the presence of close-up walls. Thus there appears to be a dynamical basis for conjectures that express the idea that number density gradients are much larger in the vertical direction than in the transverse directions (see figure 7 in Fortes *et al.* 1987). However, the extended cross-stream alignments of single lines of spheres which are evident in two dimensions, do not seem to occur in three. Evidently single lines of particles which are not constrained to move in two dimensions are unstable. There is nonetheless a visible flow-induced anisotropy favouring cross-stream alignment in three-dimensional beds. Admittedly this is a conjecture based on casual observation needing verification which, if true, is true in to-be-determined limits.

In this paper we confine our attention to the observed stability of the line of spheres which are constrained to move in two dimensions between parallel plates. The lines of particles shown in figures 1 and 2 were stable in the sense that they could be maintained for long times; in the best cases for hours. More typically these lines break up minutes after forming. We were not able to precisely assess the effects on the stability of the arrays of the unwanted eddying in the bed produced at the distributor and perhaps of other causes.

The numerical simulation in this paper is meant to model our observations of stable cross-stream arrays of spheres. We do this in a strictly two-dimensional

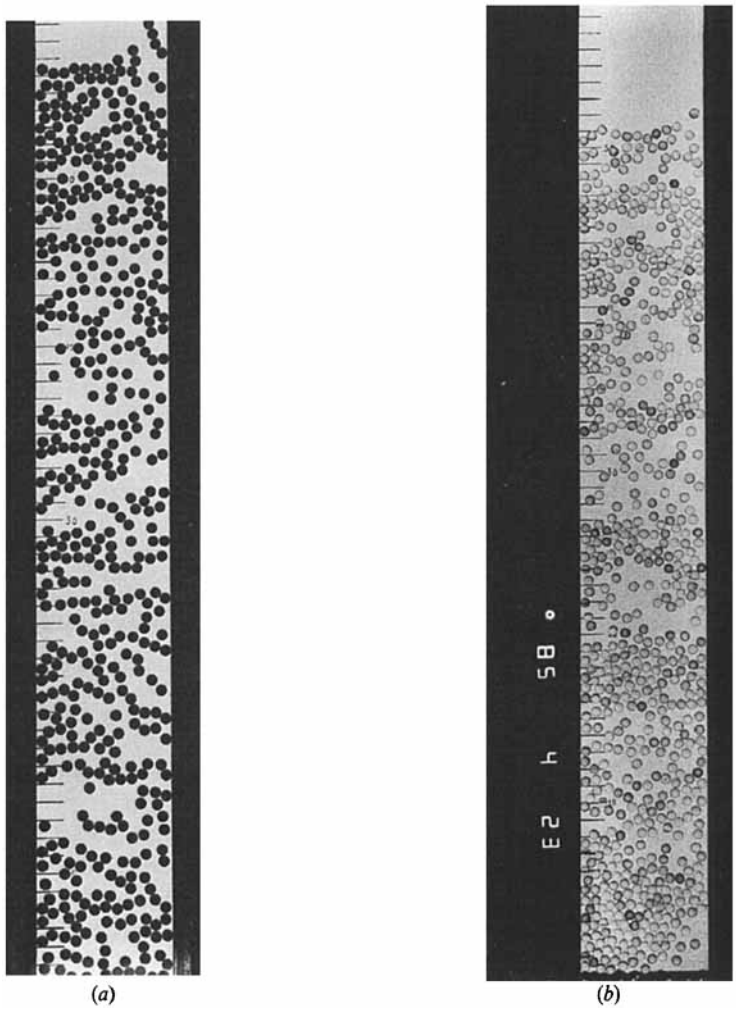

FIGURE 3. A fully expanded two-dimensional bed of spheres. The one-dimensional nature of the particle density is apparent. (*a*) Plastic spheres, $R = 305$. (*b*) Glass spheres, $R = 1700$.

approximation of flow past an array of cylinders which are arranged with their lines of centres perpendicular to the stream. The array lives in $\mathbb{R}^2$ without boundaries. The flow is assumed to be laminar and is computed for Reynolds numbers up to 100. We use a time-dependent Navier–Stokes code following the method of Bristeau, Glowinski & Periaux (1987). We get steady solutions from this code when the Reynolds number is of the order 100 or less depending on the aspect ratio. In fact the flow is already unsteady at much smaller Reynolds numbers in an experimental situation.

Our method for judging stability from a steady simulation is based on an examination of the forces on the cylinders. We think of the periodic array, evenly spaced, all in line, as our basic flow and we count a perturbation stable when the forces on the cylinders act to restore the basic flow. In fact we do find such stability when the distance between cylinders is not too great, and the perturbation is not too large (see §6 for a full discussion). We see greater stability at higher Reynolds numbers. These results appear to be in good agreement with observations. In

reservation, we must note that the simulation is only a weak representation of the observed flow. Spheres are different to cylinders and the flow is not steady even at moderately low values of Reynolds number because of vortex shedding (see figure 2). Moreover the perturbations which are prescribed in the simulation, the aspect ratio and stagger ratio, are not prescribed in experiments and instead are determined by the motion. The Reynolds numbers ($\leqslant 100$) for which our simulations were done are smaller than the Reynolds number (≈ 300) for our experiments. In experiments the Reynolds number is determined by the requirement that the drag acting on the sphere balances its weight, and smaller Reynolds numbers could presumably be obtained by using lighter spheres. It is necessary to add that we are talking about different Reynolds numbers; our simulation is done for an array of cylinders, not spheres confined between two parallel plates.

The problem of the stability of arrays of spheres in Stokes' flow has been considered by Crowley (1971) and Goren (1983). A one-dimensional array of spheres in Stokes' flow was shown to be unstable by Crowley. He accounted for the interparticle interactions by making a first-order correction to Stokes' drag in terms of d/b, where d is the diameter of spheres and b is the interparticle spacing. This is consistent with the present calculations which show that an array of cylinders is stabilized nonlinearly. Crowley also did experiments which demonstrate that the viscous instability tends to cluster the spheres into groups of three. On the other hand, experiments at higher Reynolds number lead to strong wake effects between pairs of spheres. Goren (1983) studied the stability of a one-dimensional array of spheres translating in the proximity of a no-slip wall for Stokes' flow. The only stable motion for the array is one where spheres move along the line of centres. When the array moves normal to the line of centres it is unstable. The degree of instability depends on the ratio h/b and the direction of motion, where h is the distance of the array from the no-slip wall and b is the interparticle distance. When spheres move towards the wall the degree of instability increases as the ratio h/b is increased, but the opposite is the case for the motion away from the wall. For the motion parallel to the wall the influence of the wall is different on different wavelengths.

We also used our code to determine some features of the wakes behind the cylinder. We find that the length of the wake increases linearly with the Reynolds number, but the thickness of the wake is not monotonic and appears to reach a limiting value depending on the aspect ratio (see §6 for a discussion).

2. Mathematical formulation

The aspect ratio α is

$$\alpha = \frac{L}{D} \quad (1 \leqslant \alpha < \infty),$$

where D is the diameter of the cylinder and L the horizontal projection of the distance between the centres of neighbouring cylinders. The out-of-line stagger ratio β is

$$\beta = \frac{\text{displacement of the particles perpendicular to the array}}{D} \quad (0 \leqslant \beta < \infty).$$

We also define the in-line stagger ratio γ as

$$\gamma = \frac{\text{in-line displacement of the alternate cylinders from the even spacing}}{D}$$

$$(0 \leqslant \gamma \leqslant \alpha - 1).$$

We define a Reynolds number based on diameter, $R = UD/\nu$. We also define the drag coefficient C_D and the lift or side-force coefficient C_L as

$$C_D = \frac{\text{drag force per unit length}}{0.5\rho U^2 D}, \quad C_L = \frac{\text{lift force per unit length}}{0.5\rho U^2 D}.$$

The flow past an array is characterized by R, the aspect ratio and the in-line and out-of-line stagger ratios. As R increases, inertial effects become more important.

We shall assume that the fluid is incompressible and satisfies the Navier–Stokes equations:

$$\frac{\partial \boldsymbol{u}}{\partial t} - \nu \Delta \boldsymbol{u} + (\boldsymbol{u}\cdot\nabla)\boldsymbol{u} + \nabla p = \boldsymbol{f}, \quad \nabla\cdot\boldsymbol{u} = 0 \quad \text{in } \Omega, \tag{1}$$

where Ω is all of the plane outside the cylinders. This problem is to be solved with given initial and boundary conditions. The flow past an array has three different types of boundaries, so we divide the boundary, Γ, into three parts

$$\Gamma = \Gamma_0 \cup \Gamma_N \cup \Gamma_s,$$

where Γ_s is the union of line segments parallel to the symmetry axis, Γ_N is the part of boundary on which the no-traction condition is to be applied, Γ_0 is the part of boundary on which the velocity is prescribed.

We must solve (1) subject to initial conditions

$$\boldsymbol{u}(\boldsymbol{x}, 0) = \boldsymbol{u}_0(\boldsymbol{x}), \quad p(\boldsymbol{x}, 0) = p_0(\boldsymbol{x}), \tag{2}$$

and boundary conditions

$$\left.\begin{aligned} &\boldsymbol{u} = \boldsymbol{g}_0 \quad \text{on} \quad \Gamma_0, \quad \boldsymbol{u}\cdot\boldsymbol{n} = \frac{\partial u_t}{\partial n} = 0 \quad \text{on} \quad \Gamma_s, \\ &\nu\frac{\partial \boldsymbol{u}}{\partial n} - \boldsymbol{n}p = \boldsymbol{g}_N \quad \text{on} \quad \Gamma_N. \end{aligned}\right\} \tag{3}$$

where $\boldsymbol{g}_N$ is the traction vector on Γ_N.

We define the usual function spaces for the finite-element method:

$$U = \{\boldsymbol{u} \in H^1(\Omega)^2; \quad \boldsymbol{u} = \boldsymbol{g}_0 \quad \text{on} \quad \Gamma_0; \quad \boldsymbol{u}\cdot\boldsymbol{n} = 0 \quad \text{on} \quad \Gamma_s\},$$

$$V = \{\boldsymbol{v} \in H^1(\Omega)^2; \quad \boldsymbol{v} = 0 \quad \text{on} \quad \Gamma_0; \quad \boldsymbol{v}\cdot\boldsymbol{n} = 0 \quad \text{on} \quad \Gamma_s\}.$$

After multiplying (1) by the weighting functions $v \in V$ and integrating by parts we get following variational formulation for the steady-state case:

$$\left.\begin{aligned} &\nu\int_\Omega \nabla\boldsymbol{u}\cdot\nabla\boldsymbol{v}\,dx + \int_\Omega \boldsymbol{v}\cdot(\boldsymbol{u}\cdot\nabla)\boldsymbol{u}\,dx - \int_\Omega p\,\mathrm{div}\,\boldsymbol{v}\,dx = \int_{\Gamma_N} \boldsymbol{v}\cdot\boldsymbol{g}_N\,ds \quad \text{for all} \quad v \in V, \\ &\int_\Omega q\,\mathrm{div}\,\boldsymbol{u}\,dx = 0 \quad \text{for all} \quad q \in L^2(\Omega). \end{aligned}\right\} \tag{4}$$

The numerical solution of Navier–Stokes equations, even for flow at low Reynolds numbers is difficult to compute because of the nonlinear term $(\boldsymbol{u}\cdot\nabla)\boldsymbol{u}$ and the incompressibility condition. These two problems are coupled in the Navier–Stokes equations. We shall decouple these two problems by using an operator splitting technique (see Bristeau *et al.*), which requires the solution of three problems in one time step. We outline the method for the semi-discretization of the problem in time (step Δt); all equations are understood in the sense of distributions. First we initialize by prescribing

$$\boldsymbol{u}^0 = \boldsymbol{u}_0, \quad p^0 = p_0,$$

where $\boldsymbol{u}_0$ and p_0 are assumed. For $n = 1, 2, \ldots$ we obtain $(\boldsymbol{u}^n, p^n)$ from $(\boldsymbol{u}^{n-1}, p^{n-1})$ in three fractional time steps $\theta\,\Delta t$, $(1-2\theta)\,\Delta t$ and $\theta\,\Delta t$. The intermediate time variables $\boldsymbol{u}^{n+\theta}$ and $\boldsymbol{u}^{n+1-\theta}$ are defined in the following steps.

$$\text{Step 1:}\quad \frac{\boldsymbol{u}^{n+\theta}-\boldsymbol{u}^n}{\theta\,\Delta t}-\zeta\nu\,\Delta\boldsymbol{u}^{n+\theta}+\nabla p^{n+\theta}=\xi\nu\,\Delta\boldsymbol{u}^n-(\boldsymbol{u}^n\cdot\nabla)\,\boldsymbol{u}^n,\quad \operatorname{div}(\boldsymbol{u}^{n+\theta})=0,$$

where $\boldsymbol{u}^{n+\theta}$ satisfies boundary conditions (3) on Γ.

$$\text{Step 2:}\quad \frac{\boldsymbol{u}^{n+1-\theta}-\boldsymbol{u}^{n+\theta}}{(1-2\theta)\,\Delta t}-\xi\nu\,\Delta\boldsymbol{u}^{n+1-\theta}+(\boldsymbol{u}^{n+1-\theta}\cdot\nabla)\,\boldsymbol{u}^{n+1-\theta}=\zeta\nu\,\Delta\boldsymbol{u}^{n+\theta}-\nabla p^{n+\theta},$$

where $\boldsymbol{u}^{n+1-\theta}$ satisfies boundary conditions (3) on Γ.

Step 3:

$$\frac{\boldsymbol{u}^{n+1}-\boldsymbol{u}^{n+1-\theta}}{\theta\,\Delta t}-\zeta\nu\,\Delta\boldsymbol{u}^{n+1}+\nabla p^{n+1}=\xi\nu\,\Delta\boldsymbol{u}^{n+1-\theta}-(\boldsymbol{u}^{n+1-\theta}\cdot\nabla)\,\boldsymbol{u}^{n+1-\theta},\quad \operatorname{div}(\boldsymbol{u}^{n+1})=0,$$

where $\boldsymbol{u}^{n+1}$ satisfies boundary conditions (3) on Γ. Next n.

The above scheme has the following properties. (i) By using the operator splitting method we have been able to decouple nonlinearity and incompressibility in the Navier–Stokes equations. (ii) Step 1 and step 3 are Stokes-like problems. (iii) Step 2 is a nonlinear problem, with no incompressibility condition attached. (iv) For the fully discretized problem with $\zeta = (1-2\theta)/(1-\theta), \xi = \theta/(1-\theta)$, the matrices of the terms with time derivatives and diffusion terms are same at each time step. (v) For a linear model problem, one can show that if $\theta = 1-1/\sqrt{2} = 0.29289$, then the scheme is second-order accurate and unconditionally stable. The nonlinear problem is solved by the least-square conjugate gradient method and the Stokes-like problem is solved by a conjugate gradient method. These methods are described by Bristeau *et al.*

The space is discretized using the pseudo P_2–P_1 elements. Let τ_h denote the triangulation of $\bar{\Omega}$. Each triangle is further subdivided into four triangles by joining the midpoints of each side. Let τ_K be the set of four subtriangles of $K \in \tau_h$. Then the pressure, p, is in the space

$$Q_h = \{q_h \in L^2(\Omega);\quad q_{h|K} \in P_1\ \forall K \in \tau_h\}$$

and the discrete velocity space, U_h, is defined as

$$U_h = W_h \cap U,$$

where

$$W_h = \{w_h \in C^0(\Omega)^2;\, w_{h|K'} \in P_1\ \forall K' \in \tau_K\ \forall K \in \tau_h\}.$$

The weighting functions are in the space

$$V_h = W_h \cap V.$$

The set containing the basis functions for the space Q_h is

$$\{\phi_s\}_{s\in\rho_h} \subset Q_h \quad \text{with} \quad \phi_s(s') = \delta_{ss'},$$

where ρ_h denotes the set of all vertices in τ_h.

Let N_h be the set of all nodes in τ_h, which includes the nodes at midside points and vertices. The set containing the basis function for the space W_h is

$$\{\boldsymbol{e}_1\phi_N, \boldsymbol{e}_2\phi_N\}_{N\in N_h} \subset W_h \quad \text{with} \quad \phi_N(N') = \delta_{NN'}$$

where $\boldsymbol{e}_1, \boldsymbol{e}_2$ are orthonormal basis vectors in $\mathbb{R}^2$.

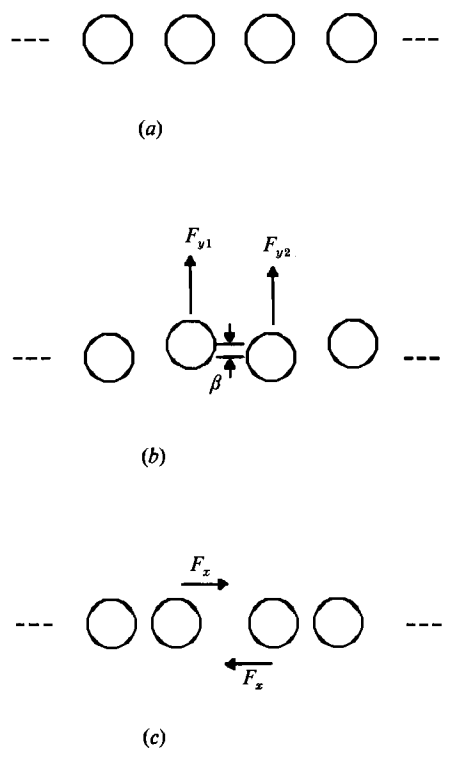

FIGURE 4. The different configurations of the arrays of cylinders for which numerical simulations were made. (*a*) In the stable configuration for the array the cylinders are all in a row but their spacing is not determined. (*b*) Alternate cylinders are displaced in the vertical direction, measured by the out-of-line stagger ratio β. (*c*) Alternate cylinders are displaced in the horizontal direction, measured by the in-line stagger ratio γ (see text for the definition of γ). The configuration (*a*) is stable when the forces on the cylinders are as drawn in (*b*) and (*c*).

3. Domain selection

The problem is to compute the flow past an array of cylinders. It is an infinite-domain problem, whereas for a numerical simulation the computational domain must be of a finite size. It is possible to approximate the conditions for large y by free-stream conditions, but no such approximation can be made for any x. This forces us to look for some symmetry to reduce the domain size in the x-direction. Along the y-direction, the flow is uniform at minus infinity, so the flow can be assumed to be approximately uniform far enough upstream. We cannot make the same assumption for the downstream boundary because of the vortices behind the cylinders; a less constrained downstream boundary condition should be used. The natural boundary conditions expressed by (3) are a natural choice for the downstream condition. The symmetric configurations which allow us to reduce the size of the computational domain and study the stability of the array are shown in figure 4. The lines of even geometric symmetry are also streamlines for a steady flow. The size of the computational domain in the horizontal direction can be limited to the region between the two lines of even symmetry, but this symmetry assumption lacks generality. Periodic conditions at the lateral boundaries may be sufficiently general. The special periodic condition with even symmetry eliminates the type of unsteady flows that we observe in our experiments at the Reynolds numbers for which the

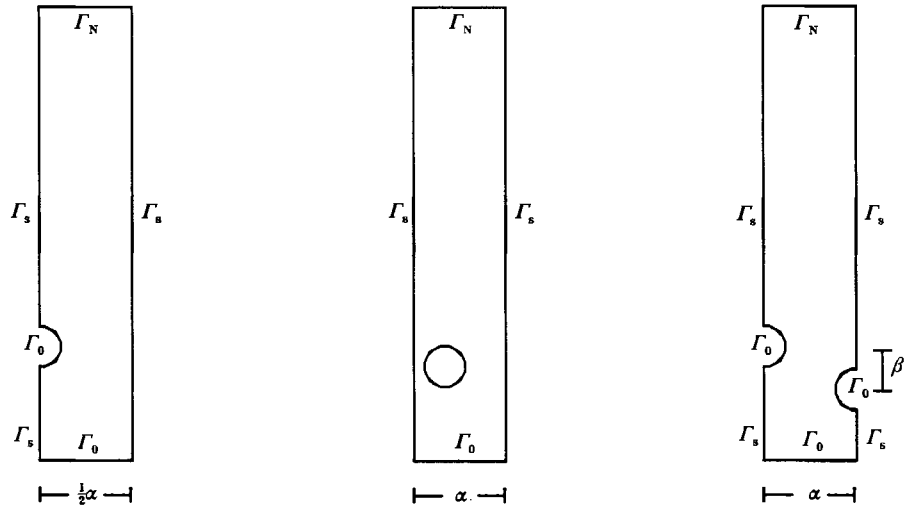

FIGURE 5. Typical computational domains. The labels attached to the boundaries indicate the type of boundary condition imposed (see (3)). (*a*) Computational domain for the stable configuration. (*b*) Computational domain for the in-line staggered arrays. (*c*) Computational domain for the out-of-line staggered arrays.

spheres could be fluidized. The computational domains for the different array configurations are shown in figure 5.

The procedure used to fix the location of downstream and upstream boundaries is the standard 'cut and try'. We say that the distance is satisfactory if results do not change significantly when boundaries are moved. For large Reynolds numbers the wake is very large, forcing the downstream boundary far downstream. The increased size of the computational domain rapidly makes the computation too expensive. This limited the range of Reynolds numbers that we could study. Methods of exponential stretching can possibly be used to handle this difficulty.

4. Convergence tests

We did convergence tests to make sure that the drag coefficient and the velocity field obtained with our numerical scheme are reliable. A typical meshed domain is shown in figure 6. For this fixed domain we increased the number of nodes by putting the additional nodes in the high-velocity-gradient areas and computed the drag coefficient acting on the two cylinders. The velocity field obtained is so close for the three cases considered that the difference cannot be noticed on the stream-function plots. The numerical convergence of the computed drag coefficient on the two cylinders is displayed in figure 7 for three different values of the Reynolds number.

5. A single cylinder in an infinite domain

The main purpose of this section is to check the accuracy of the results obtained using our code. In figure 8 we compare our calculation of the drag coefficient on a single cylinder in an array with a very large aspect ratio ($\alpha = 28$) with calculations of the drag coefficient on a single cylinder in an unbounded domain by Fornberg

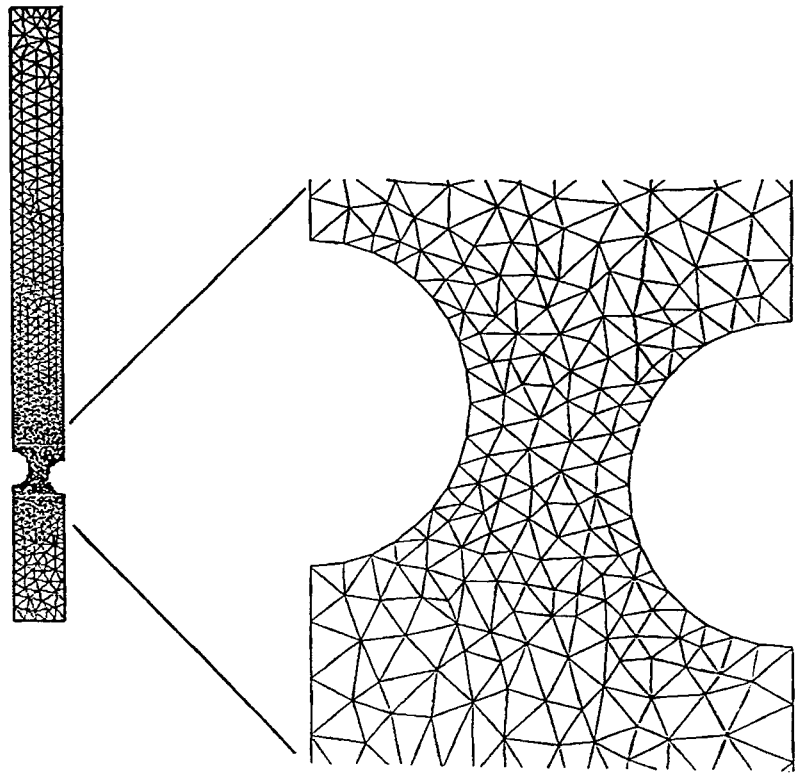

FIGURE 6. A typical mesh used for computation. Pressure elements are shown. The number of nodes is 2100.

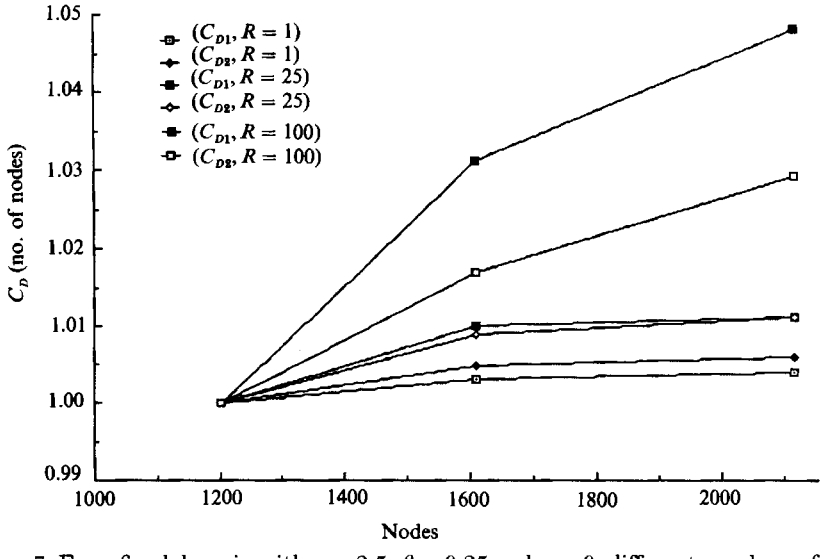

FIGURE 7. For a fixed domain with $\alpha = 2.5$, $\beta = 0.25$ and $\gamma = 0$, different numbers of nodes are used to solve the same problem. Let,

$$C_{Di}\,(\text{no. of nodes}) = \frac{C_{Di}\,(\text{no. of nodes}) - C_{Di}\,(\text{no. of nodes} = 1200)}{C_{Di}\,(\text{no. of nodes} = 1200)}.$$

C_{D1} and C_{D2} are plotted as a function of the number of nodes for three different values of Reynolds number. The numerical convergence deteriorates with Reynolds number.

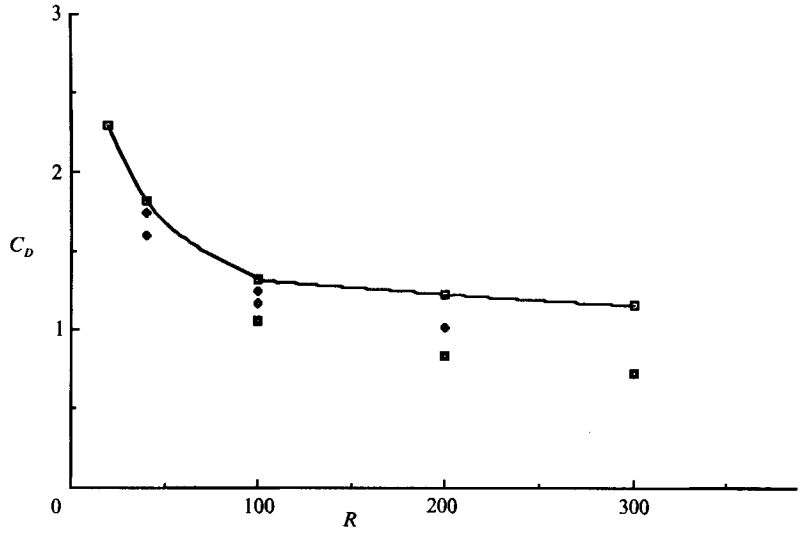

FIGURE 8. The drag coefficient versus Reynolds number for an isolated cylinder. ⊡, Experimental; ◆, present study; □, Fornberg (1985); ◇, Braza *et al.* (1986).

(1985) and Braza, Chassaing & Ha Minh (1986) and with the known experimental values. The length and width of the wake closely matches the known results for flow past a single cylinder obtained by Fornberg. To make sure that the side boundaries are far enough away we tried different domains. At $R = 100$, $C_D = 2.986$ for $\alpha = 2.5$, $C_D = 1.291$ for $\alpha = 14$ and $C_D = 1.240$ for $\alpha = 28$. From figure 8 and the results just mentioned we conclude that the computed drag coefficient is correct and it is converging towards the case of flow past a single cylinder, and the code is expected to give correct results for the flows past arrays.

6. Results

6.1. *Stability of a horizontal array*

The array is stable for both in-line and out-of-line displacement of the cylinders from the basic stable configuration under certain conditions.

6.1.1. *Stability of the array under out-of-line perturbation of the cylinders*

The drag force acting on a cylinder is a function of the aspect ratio, out-of-line stagger ratio and Reynolds number:

$$C_{Di} = C_{Di}(\alpha, \beta, R, \gamma); \quad \gamma = 0 \quad (i = 1, 2),$$

where C_{D1} and C_{D2} are the drag coefficient acting on the upper and lower cylinders respectively in the vertical direction as shown in figure 4(*b*). The diameter of the cylinders is taken to be one.

For the array to be stable, the drag coefficient acting on the lower cylinder should be larger than the drag coefficient acting on the upper cylinder. To quantify this stabilizing effect, we define a non-dimensional stabilizing force

$$\Delta C_D = \frac{C_{D2} - C_{D1}}{C_D} = \frac{F_{y2} - F_{y1}}{F_y},$$

where $C_D = \frac{1}{2}(C_{D2} + C_{D1})$, and $F_y = \frac{1}{2}(F_{y2} + F_{y1})$ is the average drag force.

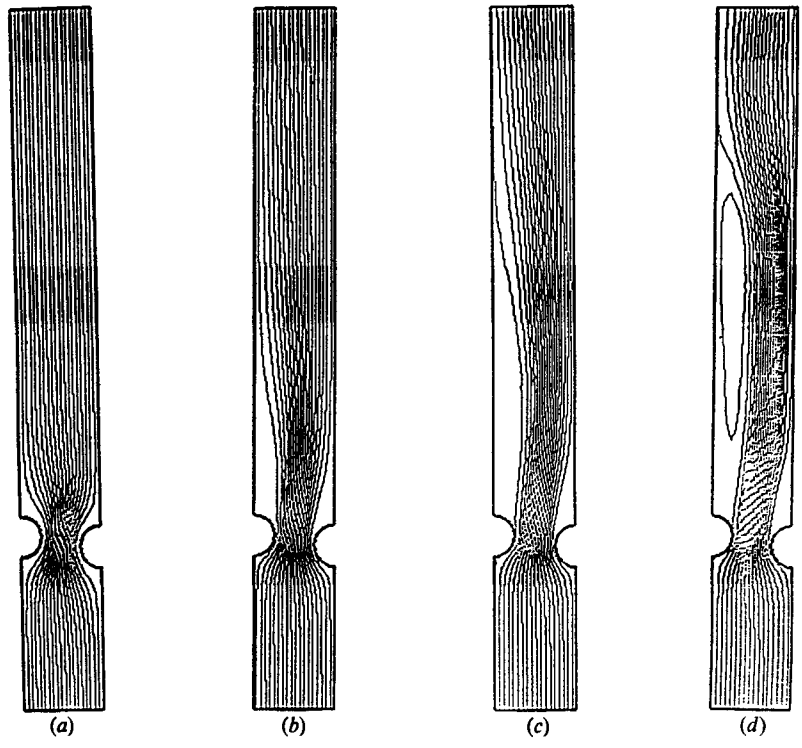

FIGURE 9. The streamlines for the flow past an array with $\alpha = 2.0$ and $\beta = 0.5$. (*a*) $R = 1$, (*b*) $R = 25$, (*c*) $R = 50$, (*d*) $R = 100$.

Again, ΔC_D is a function of the aspect ratio, the out-of-line stagger ratio and the Reynolds number. The streamlines for the flow are shown in figure 9 for different values of the Reynolds number. Table 1 shows the variation of C_{Di} and ΔC_D with the parameters. From this table we draw the following conclusions: (*a*) ΔC_D decreases with an increase in α; (*b*) ΔC_D is maximum for some value of β; (*c*) ΔC_D increases with R, for the range of Reynolds numbers studied.

One can understand the stabilizing effect in terms of the position of the separation points. Let θ be the angle of a point on the surface of the cylinder from the negative y-direction, the upstream direction. The flow separates at $\theta = \theta_s$. The separation angle θ_s on a cylinder in the array is larger than 90° in all the cases we have considered. When the cylinders are staggered out-of-line, the positions of the separation points change relative to their positions in the stable configuration, moving forward (upstream) on the cylinders in the upper row and rearward (downstream) on the cylinders in the lower row. When the separation point on the upper cylinder moves forward towards $\theta = 90°$ there is a decrease in the drag because the region of high shear stress becomes smaller. Similarly, when the separation point on the lower cylinder moves rearward away from $\theta = 90°$ there is an increase in the drag because the region of high shear stress becomes larger. This produces stabilizing forces which appear to be responsible for the stability of the array. This movement in the location of the separation point also results in a larger wake behind the upper cylinder and a smaller wake behind the lower cylinder. Figure 10 shows that the pressure recovery is larger on the lower cylinder than on the upper cylinder because flow separates at a larger angle. The larger pressure recovery on the lower cylinder

		$Re_D = 0.1$			$Re_D = 1.0$			$Re_D = 25.0$		
α	β	C_{D1}	C_{D2}	$100\Delta C_D$	C_{D1}	C_{D2}	$100\Delta C_D$	C_{D1}	C_{D2}	$100\Delta C_D$
1.5	0	—	—	—	153.84	153.86	0.01	9.103	9.103	0
1.5	0.1	1500.6	1503.1	0.17	149.84	150.64	0.53	8.465	9.516	12.42
1.5	0.25	1393.0	1393.2	0.01	138.40	140.17	1.27	7.487	9.19	22.75
1.5	0.5	—	—	—	106.56	109.26	2.53	—	—	—
1.5	1.5	—	—	—	33.16	33.15	−0.04	—	—	—
2.0	0.25	507.9	508.3	0.08	50.87	51.27	0.8	3.371	3.781	12.16
2.0	0.5	—	—	—	20.82	20.79	−0.14	—	—	—

		$Re_D = 50.0$			$Re_D = 100.0$		
α	β	C_{D1}	C_{D2}	$100\Delta C_D$	C_{D1}	C_{D2}	$100\Delta C_D$
1.5	0	6.638	6.621	−0.256	5.157	5.153	−0.08
1.5	0.1	6.086	7.136	17.25	4.764	5.651	18.62
1.5	0.25	—	—	—	4.084	5.251	28.57
1.5	0.5	—	—	—	—	—	—
1.5	1.5	—	—	—	—	—	—
2.0	0.25	2.409	2.862	18.8	1.866	2.267	21.49
2.0	0.5	—	—	—	—	—	—

TABLE 1. The stabilizing force is tabulated for different Reynolds numbers and aspect ratios for different displacements from the stable configurations

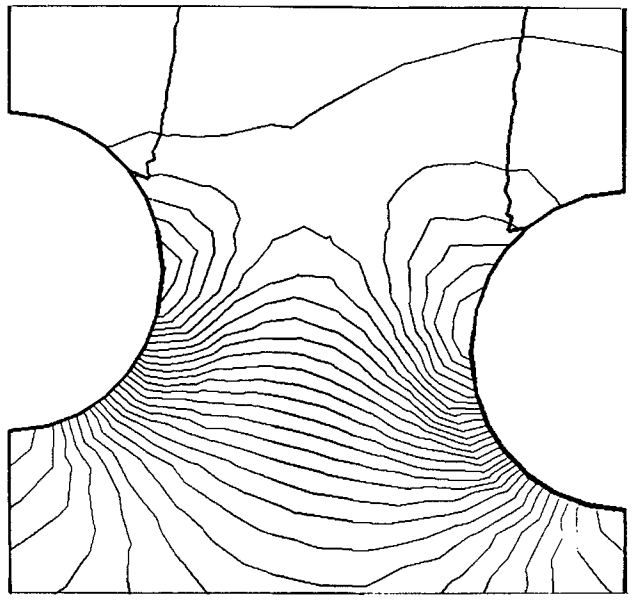

FIGURE 10. Isobars for the array with $\alpha = 2.0$, $\beta = 0.25$ and $\gamma = 0$; $R = 100$. The dark solid lines are used to show the wake bubbles. Note that the flow separates at a point downstream of the point where the adverse pressure gradient starts.

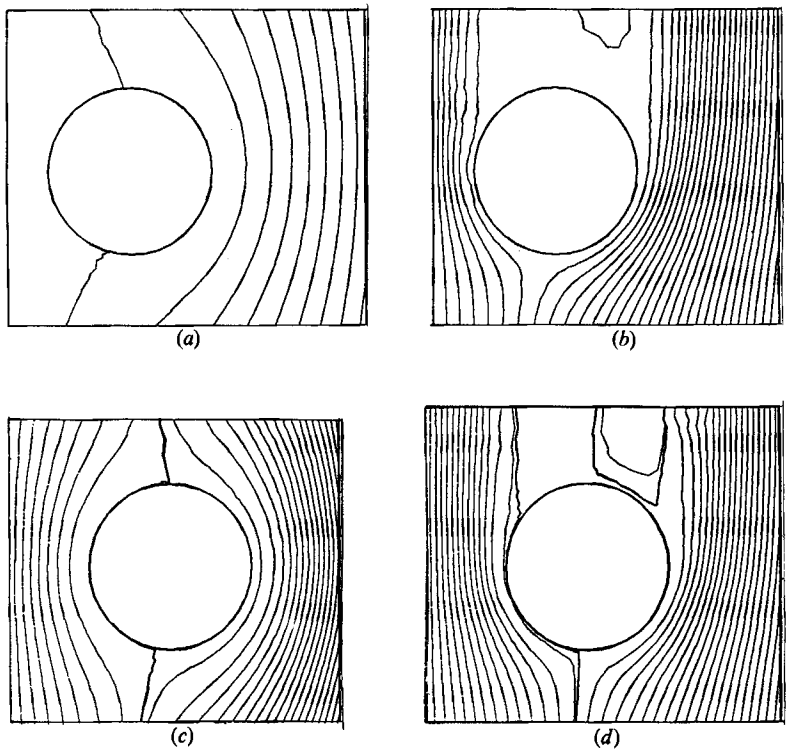

FIGURE 11. The streamlines for the flow past in-line staggered arrays, $\alpha = 2.5$, $\beta = 0$. The stagnation points are shown. A point of separation is shown in (c). (a) $R = 1$, $\gamma = 0.5$. (b) $R = 100$, $\gamma = 0.5$. (c) $R = 1$, $\gamma = 0.25$. (d) $R = 100$, $\gamma = 0.25$.

reduces the pressure drag, which is destabilizing, but this destabilizing contribution is much smaller than the stabilizing contribution that comes from the skin-friction drag. As the Reynolds number is decreased the stabilizing force decreases (conclusion *c* above). In the limit of Stokes flow there will not be any stabilizing force, $\Delta C_D = 0$.

6.1.2. *Stability of the array under in-line perturbations of even spacing*

The side force acting on a cylinder is a function of the aspect ratio, in-line stagger ratio and the Reynolds number:

$$\Delta C_L = C_L(\alpha, \beta, R, \gamma); \quad \beta = 0,$$

where C_L is the side force coefficient acting on the cylinders as shown in figure 4(*c*). When the spacing between the particles is not uniform the period cell required for the computations is doubly connected. We considered two different in-line staggered configurations which are shown in figure 11. In-line staggering displaces the forward stagnation point towards the nearer cylinder on the left side (see figure 11). This fore-and-aft asymmetry creates a strong repulsion force between the cylinders, which is stronger when γ is larger (figure 12). Moreover, the forward stagnation point creeps towards the symmetry position ($\theta = 0$) as the Reynolds number increases, as can be seen from figure 11. In figure 12 we have plotted the lift coefficient, giving the side force. The lift coefficient arises as a viscous effect, is greatest at low Reynolds numbers and is greater for more staggered arrays with closely spaced cylinders at

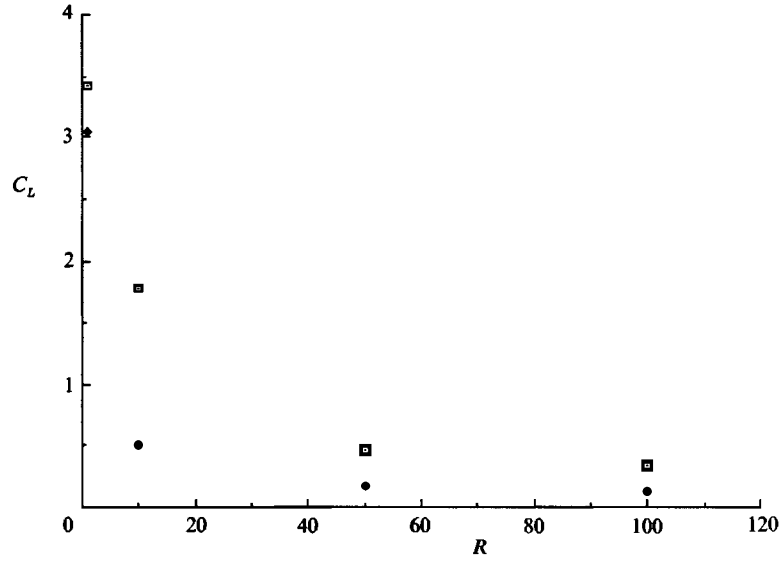

FIGURE 12. Lift-force coefficient as a function of Reynolds number on staggered configurations. ⊡, $\alpha = 2.5$, $\beta = 0$, $\gamma = 0.5$; ◆, $\alpha = 2.5$, $\beta = 0$, $\gamma = 0.25$.

fixed small Reynolds numbers. The side force arises from viscosity as in lubrication theory where the side forces support the load. This viscous effect competes with an opposing inertial effect that is best understood as a Bernoulli suction. We may conclude that even spacing is the only possibility for stability. The property of reversibility of Stokes flow implies that the sign of the force should change with the sign of velocity. Hence $F_x = 0$ for Stokes flow.

6.2. *Variation in the length and width of the wake with the aspect ratio*

Let $\theta = \theta_s$ be the separation angle. For a single cylinder in an infinite domain there is no separation for low Reynolds numbers. As R is increased past the critical value at which separation begins, the separation angle decreases monotonically from 180° to about 78°. At $R = 100$, $\theta \approx 117°$. This results in a huge wake behind the cylinder. The flow past an array is similar to flow in a converging–diverging channel. Separation is suppressed in the converging part of the channel if the channel is narrow enough. Hence the flow through an array of cylinders of small aspect ratio is not expected to separate for angles smaller than 90°. Therefore we expect that the wake behind a cylinder in an array will be smaller than the wake behind a single cylinder.

The point of separation is determined by the curvature of the channel, the Reynolds number and the rate of change of area of the channel. As the interparticle distance is increased, the rate of change of area of the channel between the two cylinders decreases, whereas the radius of curvature of the channel wall remains fixed. Hence an increase of interparticle distance will decrease the angle at which the flow separates. In the limit, this problem degenerates to the flow past a single cylinder, and flow can separate even at angles smaller than 90° for very large Reynolds numbers. This argument is supported by table 2, which gives the variation of the separation angle with aspect ratio for a fixed Reynolds number. Table 2 also shows the variation of the wake length and width with aspect ratio. For large values

α	θ	wake width	wake length
2.5	126.5	0.55	2.82
14.0	118.0	0.65	4.12
28.0	117.0	0.69	5.20

TABLE 2. The separation angle and the length and width of the wake are shown as a function of α. $R = 100$

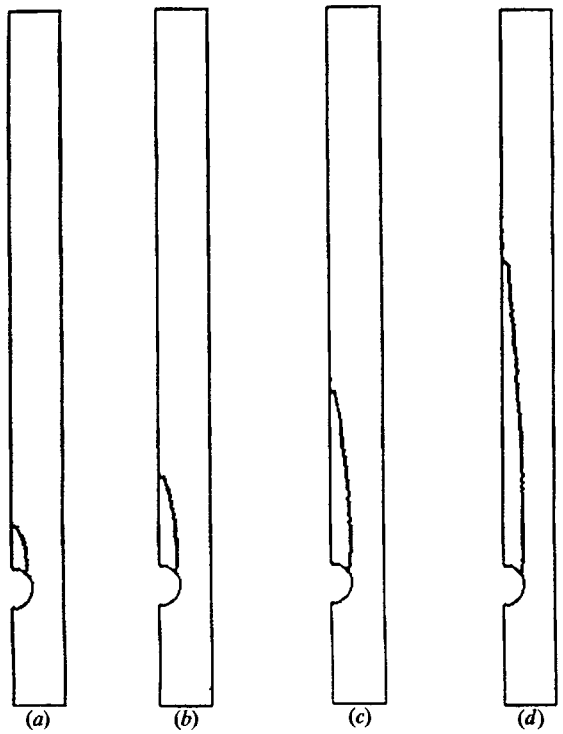

FIGURE 13. The wake bubble is shown for a basic flow configuration $\alpha = 2.5$, $\beta = 0$. (*a*) $R = 25$, (*b*) $R = 50$, (*c*) $R = 100$, (*d*) $R = 200$.

of the aspect ratio the length and width of the wake matches known results for flow past a single cylinder obtained by Fornberg (1985).

6.3. *Variation in the length and width of the wake with Reynolds number*

The wakes behind an out-of-line staggered array of cylinders are shown in figure 9 for different Reynolds numbers. The wakes behind an evenly spaced in-line array are exhibited in figure 13. The separation angle is greater than 90°. As the Reynolds number is increased from low values, first both the length and width start to grow since the separation point moves upstream. But after a certain value of the Reynolds number, which depends on the aspect ratio, the position of the separation point reaches an asymptotic value increasingly independent of the Reynolds number (see figure 14). This puts an upper limit on the maximum value of the wake width and reduces the rate of change of wake length with Reynolds number. The wake length continues to grow linearly with Reynolds number but the rate of growth at large Reynolds numbers is smaller than that at low Reynolds numbers. Also, the rate of

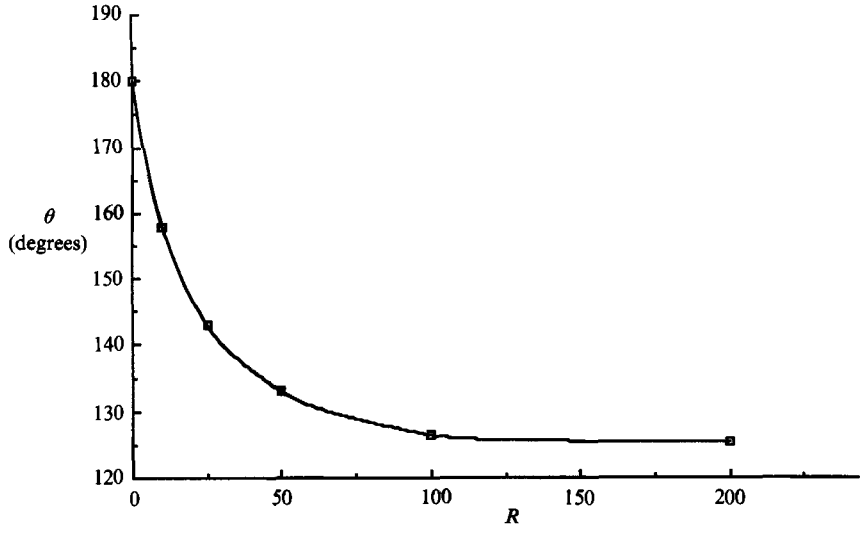

FIGURE 14. The angle of separation versus Reynolds number for an array with aspect ratio 1.25.

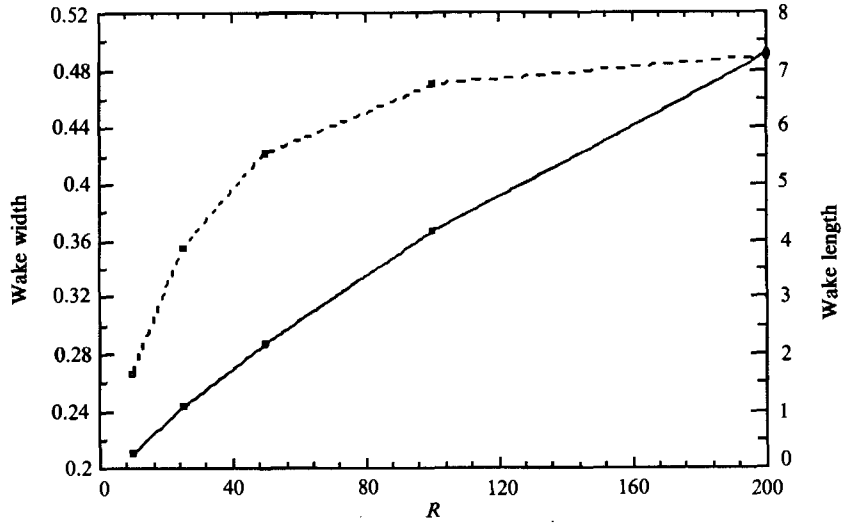

FIGURE 15. $\alpha = 1.25$. The wake length (——) and width (– – –) are plotted as a function of Reynolds number.

growth of the wake length with Reynolds number is much smaller than in the case of a single cylinder in an infinite domain. These results are shown in figure 15.

The wakes behind a periodic array of cylinders have some features in common with wakes studied by Milos & Acrivos (1987). They studied flow behind a periodic array of flat plates orthogonal to the flow with assigned velocity profiles between the plates which could be varied between uniform and fully developed flow. When they assigned a velocity profile near to the one that might be expected between cylinders with an aspect ratio $\alpha \leqslant 3.5$, they found that the recirculation region grew linearly and with R, for all R computed by them. For $4 < \alpha < 5$ growth occurred, but only up to some critical Reynolds number. The similarity between our problem and theirs

may be superficial since their assignment of velocity profiles at the entrance does not allow for the natural hydrodynamic development of streamwise variations of the velocity field between the plates. The flow through a periodic array of flat plates in which the uniform velocity is assigned far upstream and far downstream would be closer to the profile studied here. We would not expect a strong correspondence between the flat plate and cylinder problem at low Reynolds numbers, because the position of the point of separation on the cylinder changes with Reynolds number and this is important in determining the length and width of wakes. On the other hand, the position of the separation point on a cylinder asymptotes to a certain value independent of the Reynolds number at high Reynolds numbers. Hence the variation of length and width of wakes behind flat plates and cylinders might be expected to be closer at high than at low Reynolds numbers.

7. Conclusions

The following conclusions are drawn on the basis of numerical simulations.

(i) The array is stable under both in-line and out-of-line small perturbations of the cylinders from the stable-even-spaced configuration.

(ii) The array is stable even for large perturbations in the in-line stagger ratio.

(iii) The stability of an array decreases with aspect ratio and increases with Reynolds number.

(iv) For small perturbations, the stabilizing force increases with the increase in the magnitude of perturbations.

(v) As Reynolds number is increased from low values the flow separates and the separation point moves upstream asymptotically towards a point that depends on the aspect ratio. This makes the wake grow at a faster rate.

(vi) The stagnation point moves upstream with the increase in the aspect ratio.

(vii) For large Reynolds numbers, the wake length increases linearly with Reynolds number.

(viii) The wake length and width increase with aspect ratio.

This research was supported under grants from the US Army, Mathematics, the Department of Energy, the National Science Foundation and the Supercomputer Institute of the University of Minnesota. The authors are thankful to Professor R. Glowinski for his valuable suggestions.

REFERENCES

Braza, M., Chassaing, P. & Ha Minh, H. 1986 Numerical study and physical analysis of the pressure and velocity fields in the near wake of a circular cylinder. *J. Fluid Mech.* **165**, 79–130.

Bristeau, M. O., Glowinski, R. & Periaux, J. 1987 Numerical methods for the Navier–Stokes equations. Applications to the simulation of compressible and incompressible flows. *Comput. Phys. Rep.* **6**, 73–187.

Crowley, J. M. 1971 Viscosity-induced instability of a one-dimensional lattice of falling spheres. *J. Fluid Mech.* **45**, 151–160.

Fornberg, B. 1985 Steady viscous flow past a circular cylinder up to Reynolds numbers of 600. *J. Comput. Phys.* **61**, 297–320.

Fortes, A., Joseph, D. D. & Lundgren, T. 1987 Nonlinear mechanics of fluidization of beds of spherical particles. *J. Fluid Mech.* **177**, 467–483.

Goren, S. L. 1983 Resistance and stability of a line of particles moving near a wall. *J. Fluid Mech.* **132**, 185–196.

JOSEPH, D. D., FORTES, A., LUNDGREN, T. & SINGH, P. 1987 Nonlinear mechanics of fluidization of beds of spheres, cylinders and disks in water. In *Advances in Multiphase Flow and Related Problems* (ed. G. Papanicolau), pp. 101–122. SIAM.

MILOS, F. S. & ACRIVOS, A. 1987 Steady flow past sudden expansions at large Reynolds number. Part II: Navier–Stokes solutions for the cascade expansions. *Phys. Fluids* **30**, 7–26.

WALLIS, G. B. 1969 *One-Dimensional Two-Phase Flow*. McGraw-Hill.